

Search for Randall-Sundrum–like model with a small curvature through photon-induced diphoton production at the LHC

S.C. İnan*

Department of Physics, Sivas Cumhuriyet University, 58140, Sivas, Turkey

A.V. Kisselev†

*A.A. Logunov Institute for High Energy Physics,
NRC “Kurchatov Institute”, 142281, Protvino, Russian Federation*

Abstract

The potential of the LHC to explore the phenomenology of the Randall-Sundrum–like scenario with one warped extra dimension and small curvature for the process $pp \rightarrow p\gamma\gamma p \rightarrow p'\gamma\gamma p'$ is examined for two forward detector acceptances, $0.015 < \xi < 0.15$ and $0.015 < \xi < 0.5$, where ξ is the fractional proton momentum loss of the incident protons. This process, going through the subprocess $\gamma\gamma \rightarrow \gamma\gamma$, is known to be one of the most clean channels. The sensitivity bounds on the 5-dimensional gravity scale have been found at the 95% C.L. for various values of the LHC integrated luminosity.

*sceminan@cumhuriyet.edu.tr

†alexandre.kisselev@ihep.ru

I. INTRODUCTION

The Standard Model (SM), which defines the fundamental particles and their interactions at the electroweak energy scale, has been proven in all experiments, including the LHC, which has been done so far. Nevertheless, scientists are still in searching for solutions of many problems that SM cannot give satisfactory a solution. The hierarchy problem, which involves the large energy gap between the electroweak scale and the gravity scale is one of these problems. The most important answers to this unexplained phenomenon can be given by beyond the SM theories which include additional dimensions. Therefore, such models have attracted great attention in recent years and many articles have been published in the literature.

At hadron colliders, inelastic collisions are generally performed and their results are examined. However, the hadron colliders can also be used as photon-photon, photon-proton colliders as applied in the Tevatron [1, 2] and LHC [3–8]. The current results which are found in these experiments are in agreement with theoretical expectations. Specifically, the LHC experiments have shown that such photon-induced processes are important for a search of new physics. The most important advantage of the photon-induced process is that it has a clean background. It's because that this process does not include a lot of QCD originating backgrounds and uncertainties resulting from proton dissociation into jets. All these backgrounds make it difficult to identify the new physics signal beyond the SM. The photon-photon collisions through the process $pp \rightarrow p\gamma\gamma p \rightarrow p'Xp'$ has very little background. Schematic diagram for this collision is shown in Fig.(1). As one can see, both protons remain intact in this exclusive process.

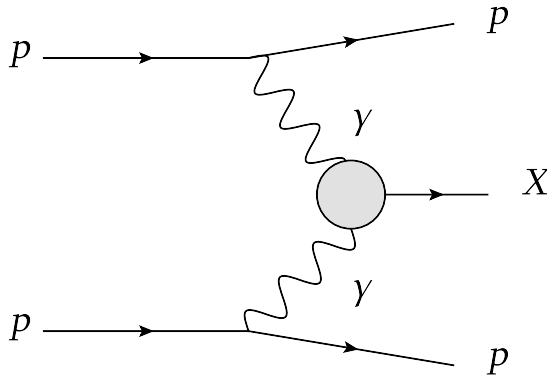


FIG. 1: Schematic diagram for the reaction $pp \rightarrow p\gamma\gamma p \rightarrow pXp$. In our case, $X = \gamma\gamma$.

Examining photon-photon interactions at the LHC is possible thanks to the plan prepared by the ATLAS Forward Physics (AFP) Collaboration and joint CMS-TOTEM Precision Proton Spectrometer (CT-PPS) [9–12]. These plans include forward detectors which are placed symmetrically at a distance from the main detectors. The forward detectors have charged particle trackers. They can catch the intact protons after elastic photon emission in the interval $\xi_{\min} < \xi < \xi_{\max}$ where ξ is the fractional proton momentum loss of the protons, $\xi = (|p| - |p'|)/|p|$. Here p is the incoming proton momentum and p' is the momentum of the intact scattered proton. The application of forward detectors to detect the scattered protons is used to identify the collision kinematics and consequently, photon-induced processes can be studied at the LHC. Forward detectors should be installed closer to the main detectors to achieve greater values of ξ .

AFP has the $0.0015 < \xi < 0.15$, $0.015 < \xi < 0.15$ detector acceptance ranges. Similarly, detector acceptance ranges of the CT-PPS are $0.0015 < \xi < 0.5$, $0.1 < \xi < 0.5$. AFP includes two types of studies. The first one is exploratory physics (anomalous couplings between γ and Z or W bosons, exclusive production, etc.). The second one is the standard QCD physics (double Pomeron exchange, exclusive production in the jet channel, single diffraction, $\gamma\gamma$ physics, etc.). The main goals of the CT-PPS experiment are the examination of the elastic proton-proton interactions, the proton-proton total cross-section and other diffractive processes. These charged particle detectors unable to determine the almost all inelastic interactions in the forward area. In this way, a very wide solid angle can be examined with the support of the CMS detector. Also, the forward detectors can be applied for precise studies [13–15]. Pile-up events can occur as a result of such high luminosity and high energy interactions. However, by using kinematics, timing constraints and exclusivity conditions, these backgrounds can be extremely restricted [16, 17]. There are many phenomenological papers in the literature which are based on the photon-induced reactions at the LHC aimed at searching for physics beyond the SM [18–41].

In the present paper we examine the Randall-Sundrum-like scenario with the small curvature (the details is given in the next section) through the main process $pp \rightarrow p\gamma\gamma p \rightarrow p'\gamma\gamma p'$ with the subprocess $\gamma\gamma \rightarrow \gamma\gamma$ in this study for the $0.015 < \xi < 0.15$ and $0.015 < \xi < 0.5$. First evidence for $\gamma\gamma \rightarrow \gamma\gamma$ scattering was observed by the ATLAS collaboration in high-energy ultra-peripheral heavy ions collisions [42]. After that, the CMS collaboration was reported for the same process [43]. Therefore, studies on this process have gained more im-

portance in recent times. Recently, we have studied the photon-induced dimuon production at the LHC [44]. Here we will do the same analysis for the diphoton production.

The processes contributing to the SM exclusive photon-photon production consist of diagrams with charged fermions (leptons, quarks), W boson loop contributions and gluon loop diagrams. Also, the interference terms of these processes should be taken into account in order to obtain the whole SM cross section.

These processes have been examined in refs. [45–49]. QCD gluon loop contributions are dominant at low energy regions whereas W loop contributions dominate at higher high energy regions. As shown in [50] QCD loop contribution can be neglected for the diphoton mass larger than 200 GeV. In our study, we have implemented the cut on the diphoton mass of 200 GeV, and therefore, we have omitted the QCD loop contributions.

There are 16 helicity amplitudes of the process $\gamma\gamma \rightarrow \gamma\gamma$. However, if T-invariance, P-invariance and Bose statistics are taken into consideration, the following relations are obtained

$$\begin{aligned}
M_{++++} &= M_{----} ; & M_{++--} &= M_{--++} ; \\
M_{+--+} &= M_{-+-+} ; & M_{+---} &= M_{-+++} ; \\
M_{++++} &= M_{+---} = M_{+--+} = M_{-+++} \\
&= M_{----} = M_{-+-+} = M_{+--+} = M_{+---} .
\end{aligned} \tag{1}$$

With using there relations, the total matrix element takes the form

$$|M|^2 = 2|M_{++++}|^2 + 2|M_{++--}|^2 + 2|M_{+--+}|^2 + 2|M_{+---}|^2 + 8|M_{+---}|^2 . \tag{2}$$

Taking into account the crossing symmetry, we find relations between amplitudes,

$$\begin{aligned}
M_{+--+}(\hat{s}, \hat{t}, \hat{u}) &= M_{++++}(\hat{u}, \hat{t}, \hat{s}) , \\
M_{+--+}(\hat{s}, \hat{t}, \hat{u}) &= M_{++++}(\hat{t}, \hat{s}, \hat{u}) = M_{++++}(\hat{t}, \hat{u}, \hat{s}) , \\
M_{+--+}(\hat{s}, \hat{t}, \hat{u}) &= M_{+--+}(\hat{s}, \hat{t}, \hat{s})
\end{aligned} \tag{3}$$

All of SM helicity amplitudes can be found in [47, 48]. Using relations $\ln(\hat{u}) = \ln(-\hat{u}) + i\pi$, $\ln(\hat{t}) = \ln(-\hat{t}) + i\pi$, $\ln(-\hat{s}) = \ln(\hat{s}) + i\pi$, the helicity amplitudes corresponding to the fermion loops can be obtained by neglecting the terms like m_f^2/\hat{s} , m_f^2/\hat{t} and m_f^2/\hat{u}

$$\frac{1}{\alpha^2 Q_f^4} M_{++++}^f(\hat{s}, \hat{t}, \hat{u}) = -8 - 8\left(\frac{\hat{u} - \hat{t}}{\hat{s}}\right) \text{Ln}\left(\frac{\hat{u}}{\hat{t}}\right) - 4\left(\frac{\hat{t}^2 + \hat{u}^2}{\hat{s}^2}\right) [\text{Ln}\left(\frac{\hat{u}}{\hat{t}}\right) \text{Ln}\left(\frac{\hat{u}}{\hat{t}}\right) + \pi^2] , \tag{4}$$

$$M_{++++}^f(\hat{s}, \hat{t}, \hat{u}) \simeq M_{++--}^f(\hat{s}, \hat{t}, \hat{u}) \simeq 8\alpha^2 Q_f^4 . \quad (5)$$

where invariant Mandelstam variables are defined as $\hat{s} = (p_1 + p_2)^2$, $\hat{t} = (p_1 - p_3)^2$ and $\hat{u} = (p_2 - p_3)^2$ and m_f , Q_f is the mass of the fermion f and its charge, respectively. The other helicity amplitudes can be obtained by using relations in Eq. (3).

It can be found the terms for W loop contribution with neglecting the m_W^2/\hat{s} , m_W^2/\hat{t} and m_W^2/\hat{u} using similar approximation,

$$\begin{aligned} \frac{1}{\alpha^2} M_{++++}^W(\hat{s}, \hat{t}, \hat{u}) &= -16i\pi \left[\frac{\hat{s}}{\hat{t}} \text{Ln}\left(\frac{-\hat{t}}{m_W^2}\right) + \frac{\hat{s}}{\hat{u}} \text{Ln}\left(\frac{-\hat{u}}{m_W^2}\right) \right] \\ &+ 12 + 12 \left(\frac{\hat{u} - \hat{t}}{\hat{s}} \right) \text{Ln}\left(\frac{\hat{u}}{\hat{t}}\right) \\ &+ 16 \left(1 - \frac{3\hat{t}\hat{u}}{4\hat{s}^2} \right) \left[\text{Ln}\left(\frac{\hat{u}}{\hat{t}}\right) \text{Ln}\left(\frac{\hat{u}}{\hat{t}}\right) + \pi^2 \right] \\ &+ 16 \left[\frac{\hat{s}}{\hat{t}} \text{Ln}\left(\frac{\hat{s}}{m_W^2}\right) \text{Ln}\left(\frac{-\hat{t}}{m_W^2}\right) + \frac{\hat{s}}{\hat{u}} \text{Ln}\left(\frac{\hat{s}}{m_W^2}\right) \text{Ln}\left(\frac{-\hat{u}}{m_W^2}\right) \right. \\ &\left. + \frac{\hat{s}^2}{\hat{t}\hat{u}} \text{Ln}\left(\frac{-\hat{t}}{m_W^2}\right) \text{Ln}\left(\frac{-\hat{u}}{m_W^2}\right) \right] , \end{aligned} \quad (6)$$

$$\begin{aligned} \frac{1}{\alpha^2} M_{+--+}^W(\hat{s}, \hat{t}, \hat{u}) &= -i\pi \left[12 \left(\frac{\hat{s} - \hat{t}}{\hat{u}} \right) + 32 \left(1 - \frac{3\hat{t}\hat{s}}{4\hat{u}^2} \right) \text{Ln}\left(\frac{\hat{s}}{-\hat{t}}\right) \right. \\ &+ 16 \frac{\hat{u}}{\hat{s}} \text{Ln}\left(\frac{-\hat{u}}{m_W^2}\right) + 16 \frac{\hat{u}^2}{\hat{t}\hat{s}} \text{Ln}\left(\frac{-\hat{t}}{m_W^2}\right) \left. \right] + 12 \\ &+ 12 \left(\frac{\hat{s} - \hat{t}}{\hat{u}} \right) \text{Ln}\left(\frac{\hat{s}}{-\hat{t}}\right) + 16 \left(1 - \frac{3\hat{t}\hat{s}}{4\hat{u}^2} \right) \text{Ln}\left(\frac{\hat{s}}{-\hat{t}}\right) \text{Ln}\left(\frac{\hat{s}}{-\hat{t}}\right) \\ &+ 16 \left[\frac{\hat{u}}{\hat{t}} \text{Ln}\left(\frac{-\hat{u}}{m_W^2}\right) \text{Ln}\left(\frac{-\hat{t}}{m_W^2}\right) + \frac{\hat{u}}{\hat{s}} \text{Ln}\left(\frac{-\hat{u}}{m_W^2}\right) \text{Ln}\left(\frac{\hat{s}}{m_W^2}\right) \right. \\ &\left. + \frac{\hat{u}^2}{\hat{t}\hat{s}} \text{Ln}\left(\frac{-\hat{t}}{m_W^2}\right) \text{Ln}\left(\frac{\hat{s}}{m_W^2}\right) \right] , \end{aligned} \quad (7)$$

$$\begin{aligned} M_{+--+}^W(\hat{s}, \hat{t}, \hat{u}) &= M_{-++-}^W(\hat{s}, \hat{t}, \hat{u}) , \\ M_{++++}^W(\hat{s}, \hat{t}, \hat{u}) &\simeq M_{++--}^W(\hat{s}, \hat{t}, \hat{u}) \simeq -12\alpha^2 . \end{aligned} \quad (8)$$

In case of $m_W^2 \ll \hat{s}$, W loop helicity amplitudes (especially, their imaginary parts) become dominant. In $m_W^2 \gg \hat{s}$ energy region fermion loop contributions are much bigger than the W loop contributions. The contribution of the top quark in all energy region is not taken into account since it is very small compared to other fermions and W loop contributions [51].

A. Photon-Photon interactions at the LHC

As it was mentioned above, it is possible to examine the photon-photon interaction with using forward detectors at the LHC. After elastic photon emission with small angles and low transverse momentum, the protons deviate slightly from their paths along the beam pipe and are probed in the forward detectors without being detected by main detectors. This deviation is related to ξ . Emitted photons which are called almost-real photons have very low virtualities. Therefore, these photons can be considered on-mass-shell. In this case, the process $pp \rightarrow p\gamma\gamma p \rightarrow p'\gamma\gamma p'$ occurs and the final state X is measured by the central detector. The value of ξ can be determined by using forward detectors. Hence, the center of mass energy of the $\gamma\gamma$ collision can be known. It is given as $W = 2E\sqrt{\xi_1\xi_2}$, where E is the energy of the incoming protons with the mass m_p . The photon-photon interaction in the hadron collision can be studied with the equivalent photon approximation (EPA) [52, 53]. The EPA includes a spectrum that depend on the photon energy ($E_\gamma = \xi E$) and photon virtuality ($Q^2 = -q^2$)

$$\frac{dN_\gamma}{dE_\gamma dQ^2} = \frac{\alpha}{\pi} \frac{1}{E_\gamma Q^2} \left[\left(1 - \frac{E_\gamma}{E}\right) \left(1 - \frac{Q_{\min}^2}{Q^2}\right) F_E + \frac{E_\gamma^2}{2E^2} F_M \right]. \quad (9)$$

The terms in above equation are defined as follows

$$Q_{\min}^2 = \frac{m_p^2 E_\gamma^2}{E(E - E_\gamma)}, \quad F_E = \frac{4m_p^2 G_E^2 + Q^2 G_M^2}{4m_p^2 + Q^2}, \quad (10)$$

$$G_E^2 = \frac{G_M^2}{\mu_p^2} = \left(1 + \frac{Q^2}{Q_0^2}\right)^{-4}, \quad F_M = G_M^2, \quad Q_0^2 = 0.71 \text{ GeV}^2. \quad (11)$$

where F_E and F_M are electric and magnetic form factors of the proton in the dipole approximation, respectively. The square of the magnetic moment of the proton is $\mu_p^2 = 7.78$. From this perspective, the resulting luminosity spectrum $\frac{dL^{\gamma\gamma}}{dW}$ is obtained as

$$\frac{dL^{\gamma\gamma}}{dW} = \int_{Q_{1,\min}^2}^{Q_{1,\max}^2} dQ_1^2 \int_{Q_{2,\min}^2}^{Q_{2,\max}^2} dQ_2^2 \int_{y_{\min}}^{y_{\max}} dy \frac{W}{2y} f_1\left(\frac{W^2}{4y}, Q_1^2\right) f_2(y, Q_2^2), \quad (12)$$

with $y_{\min} = \max(W^2/(4\xi_{\max}E), \xi_{\min}E)$, $y_{\max} = \xi_{\max}E$, $f = \frac{dN}{dE_\gamma dQ^2}$, $Q_{\max}^2 = 2 \text{ GeV}$. The contribution of more than this Q_{\max}^2 value is negligible to the integral. In Fig. 2, we show

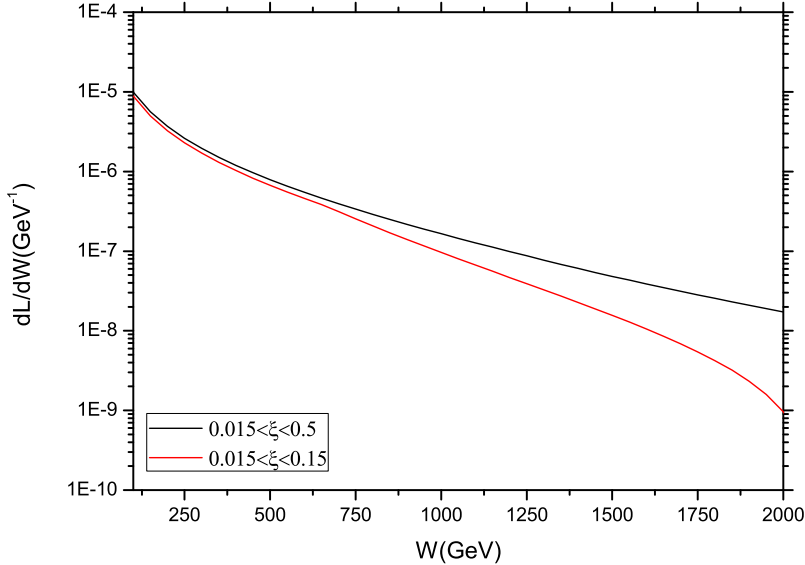


FIG. 2: Effective $\gamma\gamma$ luminosity as a function of the invariant mass of the two photon system. Figure shows the effective luminosity for two forward detector acceptances, $0.015 < \xi < 0.5$ and $0.015 < \xi < 0.15$.

the effective $\gamma\gamma$ luminosity as a function of W for $0.015 < \xi < 0.5$ and $0.015 < \xi < 0.15$. Using the Eq. 12 the total cross section for the $pp \rightarrow p\gamma\gamma p \rightarrow p'\gamma\gamma p'$ can be given as follows

$$d\sigma = \int \frac{dL^{\gamma\gamma}}{dW} d\hat{\sigma}_{\gamma\gamma \rightarrow \gamma\gamma}(W) dW, \quad (13)$$

where $d\hat{\sigma}_{\gamma\gamma \rightarrow \gamma\gamma}(W)$ is the cross section of the subprocess $\gamma\gamma \rightarrow \gamma\gamma$.

II. RANDALL-SUNDRUM-LIKE MODEL WITH A SMALL CURVATURE

One of promising possibilities to go beyond the SM is to consider a scenario with extra spatial dimensions (EDs). A framework with EDs is motivated by the (super)string theory [54]. One of the main goals of such theories is to explain the hierarchy relation between electromagnetic and Planck scales. In the model proposed by Arkani-Hamed, Dimopolous, Dvali and Antoniadis [55]–[57], called ADD, the hierarchy relation looks like

$$\bar{M}_{\text{Pl}}^2 = V_d M_D^{d+2}, \quad (14)$$

where $V_d = (2\pi R_c)^d$ is the volume of the compactified extra dimensions with the size R_c , $\bar{M}_{\text{Pl}} = M_{\text{Pl}}/\sqrt{8\pi}$ is the reduced Planck mass, and M_D is the fundamental gravity scale in

$D = 4 + d$ dimensions. The masses of the Kaluza-Klein (KK) gravitons in the ADD model are

$$m_n = \frac{n}{R_c}, \quad n = \sqrt{n_1^2 + n_2^2 + \dots + n_d^2}, \quad (15)$$

where $n_i = 0, 1, \dots$ ($i = 1, 2, \dots, d$). Thus, in the scenario with large EDs the mass splitting $\Delta m_{KK} = 1/R_c$ is very small.

However, this solution of the hierarchy problems in the ADD model cannot be considered satisfactory, since formula (14) explains a large value of the Planck mass by introducing new large scale, the volume of EDs. To overcome this shortcoming, the model with one warped extra dimension and two branes, known as RS1, was proposed by Randall and Sundrum [58].

The RS1 model is described by the following background warped metric

$$ds^2 = e^{-2\sigma(y)} \eta_{\mu\nu} dx^\mu dx^\nu - dy^2, \quad (16)$$

where $\eta_{\mu\nu}$ is the Minkowski tensor with the signature $(+, -, -, -)$, and y is an extra coordinate. The periodicity condition $y = y + 2\pi r_c$ is imposed, and the points (x_μ, y) and $(x_\mu, -y)$ are identified. As a result, we have a model of gravity in a slice of the AdS_5 space-time compactified to the orbifold S^1/Z_2 . The orbifold has two fixed points, $y = 0$ and $y = \pi r_c$. Two branes are located at these points (called Planck and TeV brane). All the SM fields are assumed to live on the TeV brane.

The classical action of the RS1 model is [58]

$$\begin{aligned} S = & \int d^4x \int_{-\pi r_c}^{\pi r_c} dy \sqrt{G} (2\bar{M}_5^3 \mathcal{R} - \Lambda) \\ & + \int d^4x \sqrt{|g^{(1)}|} (\mathcal{L}_1 - \Lambda_1) + \int d^4x \sqrt{|g^{(2)}|} (\mathcal{L}_2 - \Lambda_2), \end{aligned} \quad (17)$$

where $G_{MN}(x, y)$ is the 5-dimensional metric, $M, N = 0, 1, 2, 3, 4$. The quantities

$$g_{\mu\nu}^{(1)}(x) = G_{\mu\nu}(x, y = 0), \quad g_{\mu\nu}^{(2)}(x) = G_{\mu\nu}(x, y = \pi r_c), \quad (18)$$

where $\mu = 0, 1, 2, 3$, are induced metrics on the branes, $\mathcal{L}_1, \mathcal{L}_2$ are brane Lagrangians, $G = \det(G_{MN})$, and $g^{(i)} = \det(g_{\mu\nu}^{(i)})$ ($i = 1, 2$). \bar{M}_5 is the reduced 5-dimensional Planck scale, $M_5/(2\pi)^{1/3}$, M_5 being the fundamental gravity scale in five dimensions. Λ is a 5-dimensional cosmological constant, while $\Lambda_{1,2}$ are brane tensions.

The warp function $\sigma(y)$ in eq. (16) obeys Einstein-Hilbert's equations. For the first time, it was derived in [58]

$$\sigma_{\text{RS}}(y) = \kappa|y|, \quad (19)$$

where κ is a parameter with a dimension of mass. It defines the curvature of the 5-dimensional space-time, $\mathcal{R} = -20\kappa^2$.

The hierarchy relation in the RS1 model is of the form [58]

$$\bar{M}_{\text{Pl}}^2 = \frac{\bar{M}_5}{\kappa} \left[1 - e^{-2\pi\kappa r_c} \right] \Big|_{\kappa\pi r_c \gg 1} = \frac{\bar{M}_5}{\kappa}. \quad (20)$$

In order this relation to be satisfied, one has to put $\bar{M}_5 \sim \kappa \sim \bar{M}_{\text{Pl}}$. It was shown that $0.01 < \kappa/\bar{M}_5 < 0.1$ [59]. As a result, experimental signature of the RS1 model is a series of heavy resonances, with masses defined by the formula

$$m_n = x_n \kappa e^{-\pi\kappa r_c}, \quad n = 1, 2, \dots, \quad (21)$$

where x_n are zeros of the Bessel function $J_1(x)$.

In Ref. [60] a general solution for $\sigma(y)$ was derived. It looks like

$$\sigma(y) = \frac{\kappa r_c}{2} \left[\left| \text{Arccos} \left(\cos \frac{y}{r_c} \right) \right| - \left| \pi - \text{Arccos} \left(\cos \frac{y}{r_c} \right) \right| \right] + \frac{\pi |\kappa| r_c}{2} - C, \quad (22)$$

where $\text{Arccos}(z)$ is a principal value of the multivalued inverse trigonometric function $\arccos(z)$, and C is y -independent arbitrary parameter. This solution (i) obeys the orbifold symmetry $y \rightarrow -y$; (ii) makes the jumps of $\sigma'(y)$ on both branes; (iii) has the explicit symmetry with respect to the branes [60].

By taking $C = 0$ in (22), we get the RS1 model (19), while putting $C = \pi\kappa r_c$, we come to the Randall-Sundrum-like scenario with a small curvature of the space-time [61, 64] (RSSC model). It was applied for describing a number of processes at the LHC [65, 66].

Let us see what the main features of the RSSC model are in comparison with the features of the RS1 model. The interactions of the KK gravitons $h_{\mu\nu}^{(n)}$ with the SM fields on the TeV brane are given by the following effective Lagrangian density

$$\mathcal{L}_{\text{int}} = -\frac{1}{\bar{M}_{\text{Pl}}} h_{\mu\nu}^{(0)}(x) T_{\alpha\beta}(x) \eta^{\mu\alpha} \eta^{\nu\beta} - \frac{1}{\Lambda_\pi} \sum_{n=1}^{\infty} h_{\mu\nu}^{(n)}(x) T_{\alpha\beta}(x) \eta^{\mu\alpha} \eta^{\nu\beta}, \quad (23)$$

where $T^{\mu\nu}(x)$ is the energy-momentum tensor of the SM fields (recall that all SM fields are confined on the TeV brane). The coupling constant in (23) is equal to

$$\Lambda_\pi = \frac{\bar{M}_5^{3/2}}{\kappa^{1/2}}. \quad (24)$$

Now the hierarchy relation takes the form

$$\bar{M}_{\text{Pl}}^2 = \frac{\bar{M}_5}{\kappa} [e^{2\pi\kappa r_c} - 1] \Big|_{\kappa\pi r_c \gg 1} = \frac{\bar{M}_5}{\kappa} e^{2\pi\kappa r_c} . \quad (25)$$

This relation should be compared with eq. (20).

The masses of the KK gravitons are proportional to the curvature parameter κ [62]

$$m_n = x_n \kappa , \quad n = 1, 2, \dots . \quad (26)$$

If we put $\kappa \ll \bar{M}_5 \sim 1$ TeV, the mass splitting will be small, $\Delta m \simeq \pi\kappa$, and we come to an almost continuous mass spectrum, similar to the mass spectrum of the ADD model (15) [55]. This is in contrast to the RS1 model, in which the gravitons are heavy resonances with masses above one-few TeV.

Let us consider the s -channel KK graviton exchange contribution to the matrix element of the subprocess $\gamma\gamma \rightarrow \gamma\gamma$ with the invariant energy $\sqrt{\hat{s}}$. It is defined by the formula

$$M_{KK} = \frac{1}{2\Lambda_\pi^2} \sum_{n=1}^{\infty} e_\gamma(p_1) e_\delta(p_2) \Gamma^{\mu\nu\gamma\delta}(p_1, p_2) \frac{B_{\mu\nu\alpha\beta}}{\hat{s} - m_n^2 + i\Gamma_n} \\ \times \Gamma^{\alpha\beta\rho\sigma}(k_1, k_2) e_\rho(k_1) e_\sigma(k_2) , \quad (27)$$

where k_i, p_i ($i = 1, 2$) are momenta of incoming and outgoing photons, while $e_\mu(k_i), e_\mu(p_i)$ are their polarization vectors. $B_{\mu\nu\alpha\beta}$ is a tensor part of the graviton propagator

$$B_{\mu\nu\alpha\beta} = \eta_{\mu\alpha}\eta_{\nu\beta} + \eta_{\mu\beta}\eta_{\nu\alpha} - \frac{2}{3}\eta_{\mu\nu}\eta_{\alpha\beta} , \quad (28)$$

Vertex functions $\Gamma^{\alpha\beta\rho\sigma}$ for $h^{(n)}\gamma\gamma$ is given by

$$\Gamma^{\alpha\beta\rho\sigma}(k_1, k_2) = -\frac{i}{2} [(k_1 \cdot k_2) C^{\alpha\beta\rho\sigma} + D^{\alpha\beta\rho\sigma}] , \quad (29)$$

where

$$C^{\alpha\beta\rho\sigma} = \eta^{\alpha\rho}\eta^{\beta\sigma} + \eta^{\alpha\sigma}\eta^{\beta\rho} - \eta^{\alpha\beta}\eta^{\rho\sigma} , \quad (30)$$

$$D^{\alpha\beta\rho\sigma} = \eta^{\alpha\beta} k_1^\sigma k_2^\rho - (\eta^{\alpha\sigma} k_1^\beta k_2^\rho + \eta^{\alpha\rho} k_1^\sigma k_2^\beta - \eta^{\rho\sigma} k_1^\alpha k_2^\beta) \\ - (\eta^{\beta\sigma} k_1^\alpha k_2^\rho + \eta^{\beta\rho} k_1^\sigma k_2^\alpha - \eta^{\rho\sigma} k_1^\beta k_2^\alpha) . \quad (31)$$

Here $\eta^{\mu\nu}$ is the metric tensor of the flat space-time in four dimensions. The coherent sum in (27) is over KK modes. The total width of the graviton with the KK number n and mass m_n is given by formula [63]

$$\Gamma_n = 0.09 \frac{m_n^3}{\Lambda_\pi^2} . \quad (32)$$

Let us concentrate on the scalar part of the sum (27) which is universal for all types of processes mediated by the s-channel exchanges of the KK gravitons. It is of the form:

$$\mathcal{S}(s) = \frac{1}{\Lambda_\pi^2} \sum_{n=1}^{\infty} \frac{1}{s - m_n^2 + i\Gamma_n}. \quad (33)$$

This sum has been calculated in Ref. [64]

$$\mathcal{S}(s) = -\frac{1}{4\bar{M}_5^3 \sqrt{s}} \frac{\sin(2A) + i \sinh(2\varepsilon)}{\cos^2 A + \sinh^2 \varepsilon}. \quad (34)$$

where

$$A = \frac{\sqrt{s}}{\kappa}, \quad \varepsilon = 0.045 \left(\frac{\sqrt{s}}{\bar{M}_5} \right)^3. \quad (35)$$

As for the contribution from the t -channel graviton exchanges, $\mathcal{S}(\hat{t})$, is was shown in [64] that the function $\mathcal{S}(t)$ is pure real for $t < 0$, $\bar{M}_5 \gg \kappa$

$$\mathcal{S}(t) = -\frac{1}{2\bar{M}_5^3 \sqrt{-t}}. \quad (36)$$

Analogously, we have for the u -channel graviton exchanges

$$\mathcal{S}(u) = -\frac{1}{2\bar{M}_5^3 \sqrt{-u}}. \quad (37)$$

The virtual KK graviton exchanges should lead to deviations from the SM predictions both in a magnitude of the cross sections and angular distribution of the final photons because of the spin-2 nature of the gravitons. For the ADD model, the pure KK graviton contribution to the matrix element of the subprocess $\gamma\gamma \rightarrow \gamma\gamma$ was calculated in [51]. Its generalization for the RSSC model looks like

$$\begin{aligned} |M_{KK}|^2 = & \frac{1}{8} \{ |\mathcal{S}(\hat{s})|^2 (\hat{t}^4 + \hat{u}^4) + |\mathcal{S}(\hat{t})|^2 (\hat{s}^4 + \hat{u}^4) + |\mathcal{S}(\hat{u})|^2 (\hat{s}^4 + \hat{t}^4) \\ & + [\mathcal{S}(\hat{s})^* \mathcal{S}(\hat{t}) + \mathcal{S}(\hat{s}) \mathcal{S}(\hat{t})^*] \hat{u}^4 + [\mathcal{S}(\hat{s})^* \mathcal{S}(\hat{u}) + \mathcal{S}(\hat{s}) \mathcal{S}(\hat{u})^*] \hat{t}^4 \\ & + [\mathcal{S}(\hat{t})^* \mathcal{S}(\hat{u}) + \mathcal{S}(\hat{t}) \mathcal{S}(\hat{u})^*] \} , \end{aligned} \quad (38)$$

where \hat{s} , \hat{t} , \hat{u} are Mandelstam variables of the subprocess $\gamma\gamma \rightarrow \gamma\gamma$, and the functions $\mathcal{S}(s)$, $\mathcal{S}(t)$, $\mathcal{S}(u)$ are defined above.

III. NUMERICAL ANALYSIS

As it was mentioned above, in the RSSC model the KK graviton spectrum is similar to that in the ADD model. That is why, in contrast to the original RS1 model, an account

of effects from EDs in the RSSC model leads to deviations from the SM in magnitudes both of differential cross sections and total cross sections for the photon-induced process $pp \rightarrow p\gamma\gamma p \rightarrow p'\gamma\gamma p'$ at the LHC. This process goes via electroweak subprocess $\gamma\gamma \rightarrow \gamma\gamma$.

Our main goal is to calculate these deviations as a function of the parameters of the RSSC model. It will enable us to set the 95% C.L. search limits for the reduced 5-dimensional Planck scale \bar{M}_5 . Let us underline that this limits don't depend (up to small power corrections $\sim \kappa/\bar{M}_5$) on a value of the second parameter of the model κ . It is an interesting feature of the RS-like scenario with the small curvature.

Since we impose the cut $W > 200$ GeV on the diphoton invariant mass, we can neglect the QCD loop contributions (see Section I). Below, to estimate the LHC search limit, we will take the cut $p_t > 300(500)$ GeV, where p_t is the final photon transverse momentum. Note that $W \geq 2p_t$ due to energy conservation. Thus, the condition $W > 200$ GeV will be automatically satisfied.

We also impose the cut $|\eta_{pp}^i| < 2.5$ on the rapidities of the final photons η_{pp}^i ($i = 1, 2$) in the c.m.s of the *colliding protons*. It is equivalent to the inequality

$$\eta_{\gamma\gamma} + |\eta_X| < 2.5, \quad (39)$$

where

$$\eta_{\gamma\gamma} = \ln \frac{W + \sqrt{W^2 - 4p_t^2}}{2p_t} \quad (40)$$

is the rapidity of the final photons in the c.m.s of *two photons*, and

$$\eta_X = \frac{1}{2} \ln \frac{\xi_1}{\xi_2} \quad (41)$$

is the rapidity of the diphoton system in the in the c.m.s of the incoming protons. If the additional cut $p_t > p_{t,\min}$ is imposed, the scattering angles of the photons in their c.m.s. are bounded as

$$|\cos \theta_{\gamma\gamma}| < \begin{cases} 0, & \text{if } |\eta_X| \geq 2.5, \\ \min \left[\sqrt{1 - \left(\frac{2p_{t,\min}}{W} \right)^2}, \tanh(2.5 - |\eta_X|) \right], & \text{if } |\eta_X| < 2.5. \end{cases} \quad (42)$$

In what follows, the LHC energy is equal to 14 TeV (i.e., the energy of the incoming protons is $E = 7$ TeV).

The results of our calculations of the differential cross sections $d\sigma/dp_t$ with the cuts mentioned above as a function of the photon transverse momenta are presented in Figs. 3

and 4 for three values of \bar{M}_5 . Our calculations have shown that the differential cross

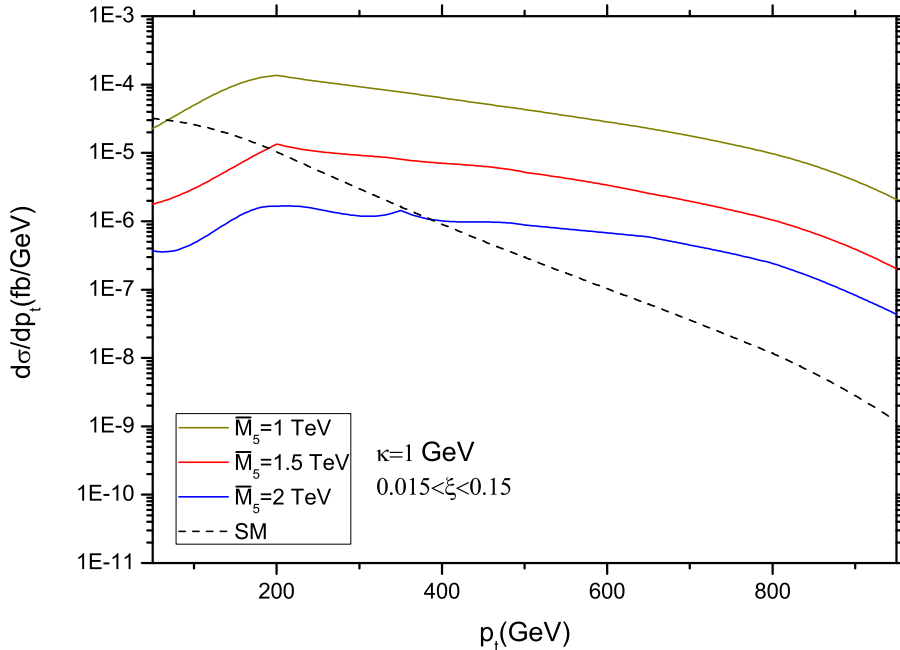


FIG. 3: The differential cross section for the process $pp \rightarrow p\gamma\gamma p$ as a function of the transverse momenta of the final photons for $\kappa = 1$ GeV and for the acceptance region $0.015 < \xi < 0.15$. The cut on the photon rapidities, $|\eta| < 2.5$, is imposed. Here and below the dotted line denotes the SM contribution.

section does not practically depend on the curvature parameter κ . The same is true for the diphoton production in photon-induced events at the LHC [44]. One can see that $d\sigma/dp_t$ exceeds the SM cross section $d\sigma_{\text{SM}}/dp_t$ for $p_t > 300$ GeV, if $0.015 < \xi < 0.15$, and for $p_t > 500$ GeV, if $0.015 < \xi < 0.5$. Moreover, the difference between $d\sigma/dp_t$ and $d\sigma_{\text{SM}}/dp_t$ increases as p_t grows. The effect is more pronounced for smaller values of \bar{M}_5 . The maximum of $d\sigma/dp_t$ around $p_t \simeq 200$ GeV (500 GeV) for the acceptance region $0.015 < \xi < 0.15$ ($0.015 < \xi < 0.5$) is a result of the integration in variable W , whose lower limit depend on p_t , as well as due to the p_t -dependence of the rapidity cut (39)–(40).

The total cross section $\sigma(p_t > p_{t,\text{min}})$ for two acceptance regions is shown in Figs. 5 and 6 as a function of the minimal transverse momenta of the final photons $p_{t,\text{min}}$. In both figures, the comparison with the pure SM predictions is given. For both acceptance regions,

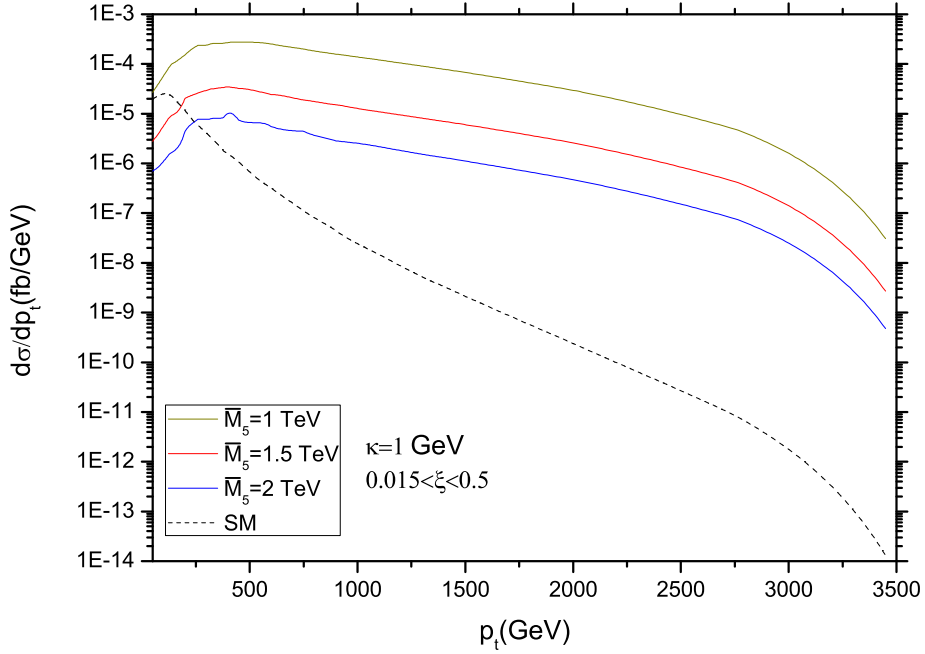


FIG. 4: The same as in Fig. 3, but for the acceptance region $0.015 < \xi < 0.5$.

a deviation of $\sigma(p_t > p_{t,\min})$ from the SM cross section $\sigma_{\text{SM}}(p_t > p_{t,\min})$ gets higher as $p_{t,\min}$ grows. The effect is more significant for $0.015 < \xi < 0.5$.

Having calculations of the total cross sections in hand, we are able to obtain the limits on \bar{M}_5 for two acceptance regions, $0.015 < \xi < 0.15$ and $0.015 < \xi < 0.5$, for $p_t > 300$ GeV and $p_t > 500$ GeV, respectively. In sensitivity analysis, we use the likelihood method from Ref. [40]. We assume that observed events follow a Poisson distribution. Then the statistics together with the prediction of the event rate leads to the following likelihood function

$$\mathfrak{L}(\sigma) = \Pr(n|b + \sigma L) . \quad (43)$$

Here n is the number of the observed events, b is the expected number of background (SM) events, σ is the total cross section, and L is the integrated luminosity. One can estimate from Figs. 5 and 6 that for the maximum luminosity value of $L = 300 \text{ fb}^{-1}$ ($L = 3000 \text{ fb}^{-1}$) when $p_t > 300$ GeV ($p_t > 500$ GeV), the expected number of the SM events is less than 0.5. Thus, we can assume that no events is observed, and put $b = 0$. Then the LHC exclusion

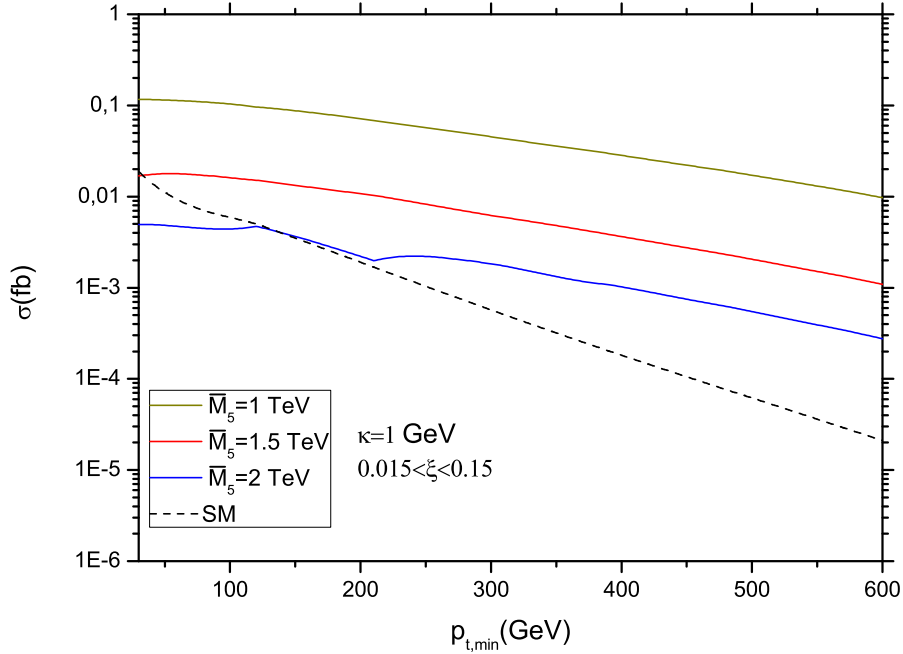


FIG. 5: The total cross section for the process $pp \rightarrow p\gamma\gamma p$ as a function of the minimal transverse momenta of the final photons $p_{t,\min}$ for the acceptance region $0.015 < \xi < 0.15$ for different values of \bar{M}_5 .

region for the credibility $1 - \alpha$ is given by the formula [40]

$$\sigma_\alpha = -\frac{1}{L} \ln(\sigma). \quad (44)$$

For the 95% C.L., which corresponds to $\alpha = 0.05$, we get from (44)

$$\sigma_{0.05} \simeq \frac{3}{L}. \quad (45)$$

First, let us consider the acceptance region $0.015 < \xi < 0.15$ and impose the cut $p_t > 300$ GeV. Using eq. (44), we have found the 95% C.L. search limits for the reduced 5-dimensional gravity scale \bar{M}_5 as a function of the integrated LHC luminosity, see Fig. 7. The analogous results for the cut $p_t > 500$ GeV are presented in Fig. 8. As one can see, for the integrated luminosity $L = 300 \text{ fb}^{-1}$, the sensitivity bounds on \bar{M}_5 are 2.01 TeV and 1.37 TeV, for the acceptance region $0.015 < \xi < 0.5$ and $0.015 < \xi < 0.15$, respectively. For $L = 3000 \text{ fb}^{-1}$ the sensitivity bounds on \bar{M}_5 are equal to 2.93 TeV and 1.74 TeV. Let us underline that

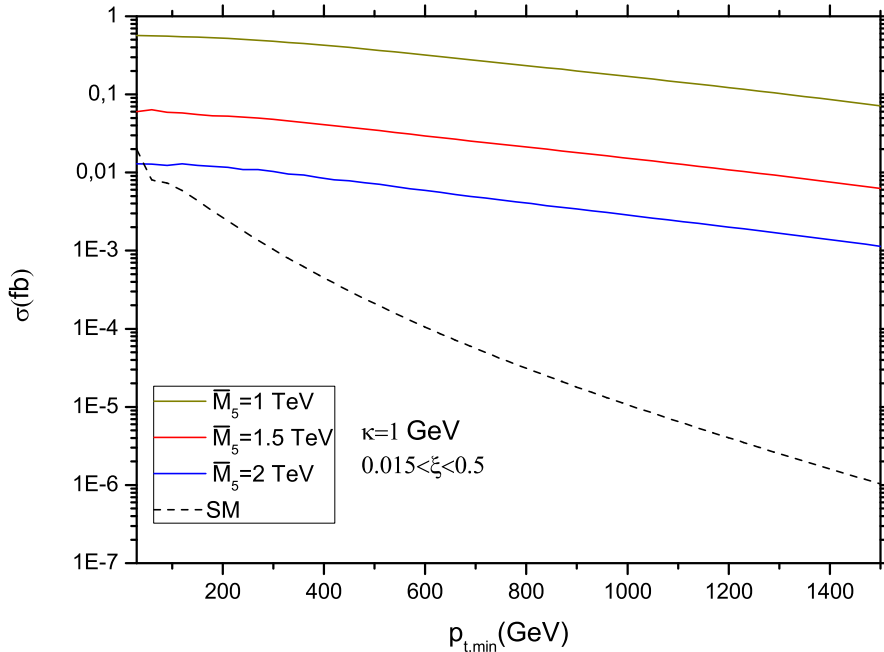


FIG. 6: The same as in Fig. 5, but for the acceptance region $0.015 < \xi < 0.5$.

these bound don't depend on the parameter κ , provided $\kappa \ll \bar{M}_5$, what is satisfied in our analysis.

Our bounds on the 5-dimensional gravity scale \bar{M}_5 are rather low in comparison with the experimental bounds on D -dimensional scale M_D in the ADD model (see, for instance,). In this regard, we must emphasize that the LHC bounds on M_D cannot be directly applied to the gravity scale \bar{M}_5 in the RSSC model. As was mentioned above (for details, see [64]), this model cannot be regarded as a small distortion of the ADD model even for very small values of the curvature κ . Moreover, in the ADD model the number of EDs should be $d \geq 2$, while in the RSSC model we deal with one ED. As for the original RS1 model, the bounds in it are put on the set of two parameters: the ratio κ/\bar{M}_5 and mass of the lightest KK graviton m_1 .

We consider the diphoton production in the photon-induced process at the LHC as a mean of looking for effects of low gravity scale \bar{M}_5 in the Randall-Sundrum-like scenario with the small curvature.

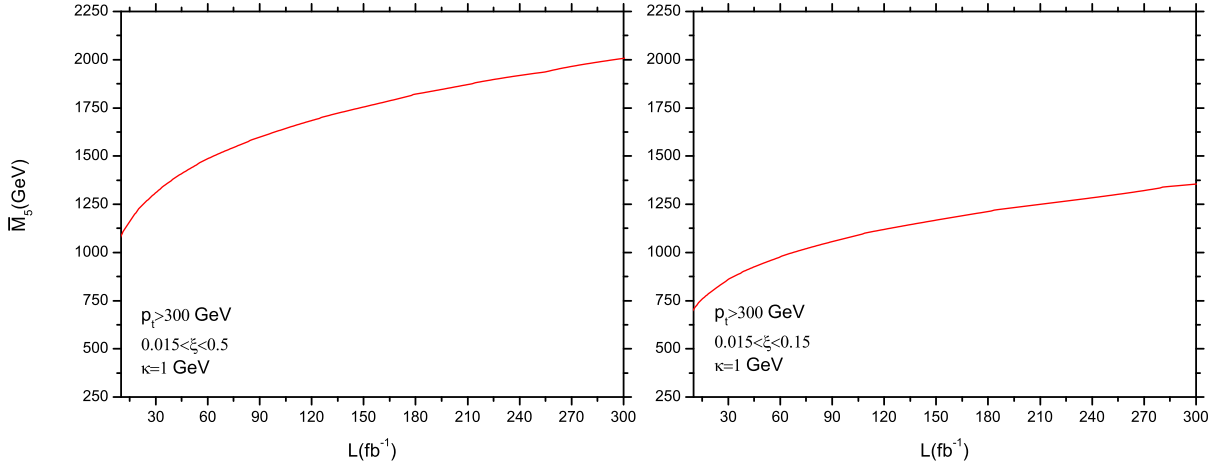


FIG. 7: The 95% C.L. search limits for the reduced 5-dimensional gravity scale \bar{M}_5 as a function of the integrated LHC luminosity with $p_t > 300$ GeV. The rapidity cut of 2.5 on the photon rapidities are imposed. Left panel: $0.015 < \xi < 0.15$. Right panel: $0.015 < \xi < 0.5$.

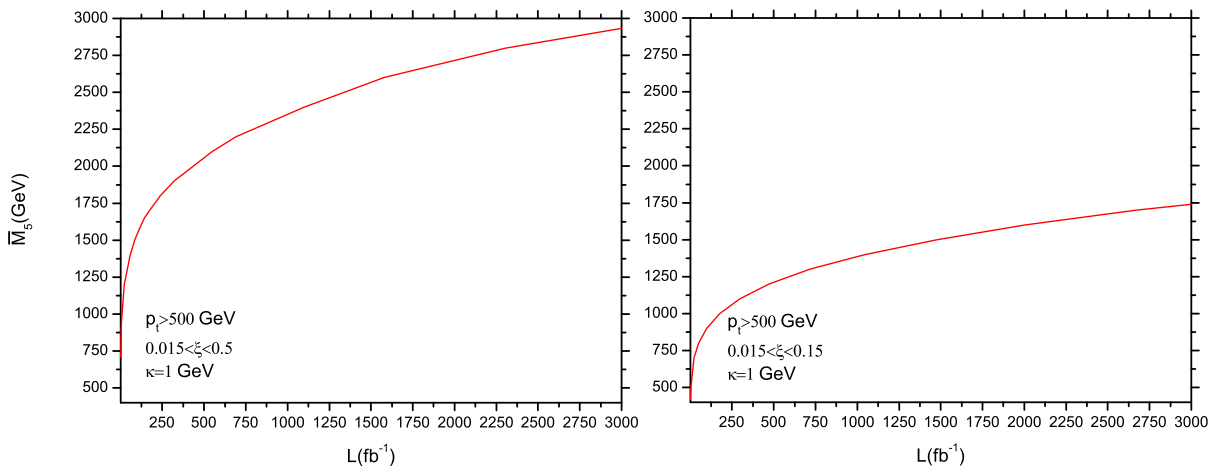


FIG. 8: The same as in Fig. 7, but for the acceptance region $p_t > 500$ GeV.

IV. CONCLUSIONS

With the forward detectors prepared by the ATLAS Forward Physics Collaboration (AFP) and CMS-TOTEM Precision Proton Spectrometer Collaboration (CT-PPS) [9–12], it becomes possible to investigate the exclusive photon-induced process $pp \rightarrow p\gamma\gamma p \rightarrow p'Xp'$ (see Fig. 1). In the present paper we have studied the diphoton production $pp \rightarrow p\gamma\gamma p \rightarrow p'\gamma\gamma p'$ at the LHC energy 14 TeV in the framework of the Randall-Sundrum-like model

with one warped ED and small curvature of the 5-dimensional space-time. The consideration was performed for two acceptance regions of the forward detector, $0.015 < \xi < 0.15$ and $0.015 < \xi < 0.5$, where ξ is the fractional proton momentum loss of the incident protons.

The distributions in the photon transverse momenta p_t with the cut $|\eta| < 2.5$ imposed on the photon rapidity η have been calculated as a function of the reduced 5-dimensional Planck scale \bar{M}_5 (see Figs. 3 and 4). It was shown that the deviation from the SM predictions gets higher as p_t grows. The total cross sections have been calculated for two acceptance regions depending on the cut imposed on the transverse momenta of the final photon, $p_t > p_{t,\min}$ (see Figs. 5 and 6). Let us underline that in the RSSC model the values of the cross sections don't depend on the curvature parameter κ , provided $\kappa \ll \bar{M}_5$, what was satisfied in our analysis. This allowed us to put the 95% C.L. search limits for \bar{M}_5 as a function of the integrated LHC luminosity (see Figs. 7 and 8). For instance, for $0.015 < \xi < 0.5$ and $p_t > 300$ GeV, this limit for \bar{M}_5 is equal to 2.01 TeV, for the integrated luminosity $L = 300$ fb⁻¹. For the HL-LHC integrated luminosity $L = 3000$ fb⁻¹ and $p_t > 500$ GeV, we have found that the 95% C.L. search limit is equal to 2.93 TeV, for the same acceptance region. In conclusion, note that recently the dimuon production in the photon-induced process at the LHC was studied in Ref. [44], in which search limits for \bar{M}_5 have been also obtained. The bounds on \bar{M}_5 in the present article are better than the bounds in [44].

-
- [1] T. Aaltonen *et al.*, (CDF Collaboration), Phys. Rev. Lett. **102**, 242001 (2009).
 - [2] T. Aaltonen *et al.* (CDF Collaboration), Phys. Rev. Lett. **102**, 222002 (2009).
 - [3] S. Chatrchyan *et al.* (CMS Collaboration), JHEP **1201**, 052 (2012).
 - [4] S. Chatrchyan *et al.* (CMS Collaboration), JHEP **1211**, 080 (2012).
 - [5] G. Aad *et al.* (ATLAS Collaboration), Phys. Lett. B **749**, 242, (2015)
 - [6] G. Aad *et al.* (ATLAS Collaboration), JHEP **08**, 009 (2016).
 - [7] M. Aaboud *et al.* (ATLAS Collaboration), Phys. Rev. D **94**, 032011 (2016).
 - [8] A. M. Sirunyan *et al.* (CMS and TOTEM Collaborations), JHEP **1807**, 153 (2018).
 - [9] ATLAS Collaboration, Tech. Rep. CERN-LHCC-2011-012. LHCC-I-020, 2011.
 - [10] L. Adamczyk *et al.*, Tech. Rep. ATLCOM-LUM-2011-006, CERN, 2011.
 - [11] L. Adamczyk, *et al.*, Tech. Rep. CERN-LHCC-2015-009. ATLAS-TDR-024, May, 2015.

- [12] M. Albrow *et al.*, CMS-TOTEM, Tech. Rep. CERN-LHCC-2014-021. TOTEM-TDR-003. CMS-TDR-13, September, 2014.
- [13] G. Antchev *et al.* (TOTEM Collaboration), EPL **96**, 21002 (2011).
- [14] G. Antchev *et al.* (TOTEM Collaboration), EPL **98**, 31002 (2012).
- [15] G. Antchev *et al.* (TOTEM Collaboration), EPL **101**, 21002 (2013).
- [16] M. Albrow *et al.* (FP420 R and D Collaboration), JINST **4**, T10001 (2009).
- [17] M.G. Albrowa, T.D. Coughlin and J.R. Forshaw, Prog. Part. Nucl. Phys. **65**, 149 (2010).
- [18] K. Piotrkowski, Phys. Rev. D **63**, 071502(R) (2001).
- [19] V. Goncalves and M. Machado, Phys. Rev. D **75**, 031502(R) (2007).
- [20] İ. Şahin and S.C. İnan, JHEP **09**, 069 (2009).
- [21] S.C. İnan, Phys. Rev. D **81**, 115002 (2010).
- [22] S. Atağ and A. Billur, JHEP **11**, 060 (2010).
- [23] İ. Şahin and A.A. Billur, Phys. Rev. D **83**, 035011 (2011).
- [24] İ. Şahin and M. Köksal, JHEP **11**, 100 (2011).
- [25] S.C. İnan and A.A. Billur, Phys. Rev. D **84**, 095002 (2011).
- [26] R.S. Gupta, Phys. Rev. D **85**, 014006 (2012).
- [27] İ. Şahin, Phys. Rev. D **85**, 033002 (2012).
- [28] L.N. Epele *et al.*, Eur. Phys. J. Plus **127**, 60 (2012).
- [29] İ. Şahin and B. Şahin, Phys. Rev. D **86**, 115001 (2012).
- [30] A.A. Billur, Europhys. Lett. **101**, 21001 (2013).
- [31] İ. Şahin *et al.*, Phys. Rev. D **88**, 095016 (2013).
- [32] H. Sun, C.X. Yue, Eur. Phys. J. C **74**, 2823 (2014).
- [33] H. Sun, Nucl. Phys. B **886**, 691 (2014).
- [34] İ. Şahin *et al.*, Phys. Rev. D **91** 035017 (2015).
- [35] M. Köksal and S.C. İnan, Adv. High Energy Phys. **2014**, 315826 (2014).
- [36] S. Fichet, G. von Gersdorff, and C. Royon, Phys. Rev. Lett. **116**, 231801, (2016).
- [37] S. Fichet, G. von Gersdorff, and C. Royon, Phys. Rev. D **93**, 075031, (2016)
- [38] S. Fichet, JHEP **1704**, 088 (2017).
- [39] C. Baldenegro *et al.*, JHEP **1706**, 142 (2017).
- [40] C. Baldenegro *et al.*, JHEP **1806**, 131 (2018).
- [41] M. Köksal *et al.*, Phys. Lett. B **783**, 375 (2018).

- [42] M. Aaboud *et al.* (ATLAS Collaboration), *Nat. Phys.* **13**, 852 (2017).
- [43] D. d’Enterria *et al.* (CMS Collaboration), arXiv:1808.03524.
- [44] S.C. İnan, A.V. Kisselev, *Eur. Phys. J. C* **78**, 729 (2018).
- [45] R. Karplus and M. Neuman, *Phys. Rev.* **83**, 776 (1951).
- [46] V. Costantini, B. De Tollis and G. Pistoni, *Nuovo Cim. A* **2**, 733 (1971).
- [47] G. Jikia and A. Tkabladze, *Phys. Lett. B* **323**, 453 (1994).
- [48] G.J. Gounaris, P.I. Porfyriadis and F.M. Renard, *Phys. Lett. B* **452**, 76 (1999) [Erratum, *ibid.* **513**, 431 (2001)].
- [49] G.J. Gounaris, P.I. Porfyriadis and F.M. Renard, *Eur. Phys. J. C* **9**, 673 (1999).
- [50] S. Fichtel, G. von Gersdorff, B. Lenzi, *et al.*, *JHEP* **1502**, 165 (2015).
- [51] S. Atağ, S.C. İnan and İ. Şahin, *JHEP* **1009**, 042 (2010).
- [52] V. Budnev, I. Ginzburg, G. Meledin and V. Serbo, *Phys. Rep.* **15**, 181 (1975).
- [53] G. Baur, K. Hencken, D. Trautmann *et al.*, *Phys. Rep.* **364**, 359 (2002).
- [54] J. Polchinski, *String theory*, Cambridge University Press, 1998, Vols. I and II.
- [55] N. Arkani-Hamed, S. Dimopoulos and G. Dvali, *Phys. Lett. B* **429**, 263 (1998).
- [56] N. Arkani-Hamed, S. Dimopoulos and G. Dvali, *Phys. Rev. D* **59**, 086004 (1999).
- [57] I. Antoniadis, N. Arkani-Hamed, S. Dimopoulos and G. Dvali, *Phys. Lett. B* **436**, 257 (1998).
- [58] L. Randall and R. Sundrum, *Phys. Rev. Lett.* **83**, 3370 (1999).
- [59] H. Davoudiasl, J.L. Hewett, and T.G. Rizzo, *Phys. Rev. D* **63**, 075004 (2001).
- [60] A.V. Kisselev, *Nucl. Phys. B* **909**, 218 (2016).
- [61] G.F. Giudice, T. Plehn and A. Strumia, *Nucl. Phys. B* **706**, 455 (2005).
- [62] A.V. Kisselev and V.A. Petrov, *Phys. Rev. D* **71**, 124032 (2005).
- [63] A.V. Kisselev, *Eur. Phys. J. C* **42**, 217 (2005).
- [64] A.V. Kisselev, *Phys. Rev. D* **73**, 024007 (2006).
- [65] A.V. Kisselev, *JHEP* **0809**, 039 (2008).
- [66] A.V. Kisselev, *JHEP* **1304**, 025 (2013).
- [67] S. Atağ, S.C. İnan and İ. Şahin, *Phys. Rev. D* **80**, 075009 (2009).
- [68] A.M. Sirunyan *et al.* (CMS Collaboration), *Eur. Phys. J. C* **78**, 789 (2018); *Phys. Rev. D* **98**, 092001 (2018).